6402 *Inorg. Chem.* **2009**, *48*, 6402–6408
DOI: 10.1021/ic8023875

Inorganic Chemistry
Article

Synthesis and Phase Width of Quaternary Selenides $Pb_4In_xM_{6-x}Se_{13}$ (M = Bi, x = 2.1−2.8; Sb, x = 2)

Ming-Fang Wang, Wen-Hen Huang, and Chi-Shen Lee*

Department of Applied Chemistry, National Chiao Tung University, 1001 University Rd., Hsinchu 30010, Taiwan

Received December 16, 2008

Quaternary selenides of $Pb_4In_xM_{6-x}Se_{13}$ (M = Bi, x = 2.1−2.8; Sb, x = 2) were synthesized by solid-state methods, and their structures were determined from X-ray diffraction of single crystals. These compounds are isostructural with $Pb_4In_2Bi_4S_{13}$ and crystallize in orthorhombic space group *Pbam* (No. 55) with Z = 4; the structure features a three-dimensional framework consisting of Z-shaped ribbon units and corner-sharing infinite one-dimensional $[InSe_4]_\infty$ chains running parallel to the c-axis, which are connected by Pb atoms to form a three-dimensional structure. Calculations of the band structure and measurements of Seebeck coefficient, electrical conductivity, and diffuse reflectance spectra confirm that these compounds are semiconductors with a narrow band gap. All compounds show semiconducting properties; the Seebeck coefficient of $Pb_4In_{2.5}Bi_{3.5}Se_{13}$ is −180 μV/K at 295 K.

Introduction

Chalcogenides that contain heavy main-group elements and exist in minerals and synthetic compounds have attracted intensive research for their prospective applications in thermoelectric devices. An effective thermoelectric material must have simultaneously a large thermoelectric power, a large electrical conductivity, and a small thermal conductivity. These properties define a thermoelectric figure of merit $ZT = (\sigma S^2/\kappa)\ T$, in which S denotes the Seebeck coefficient or thermopower, σ electrical conductivity, κ thermal conductivity, and T temperature.[1] Chalcogenides that can maintain those properties approach the case of $Bi_{2-x}Sb_xTe_{3-y}Se_y$[1] alloy, a commercial thermoelectric material with an optimized ZT near unity about 300 K. Two materials, $CsBi_4Te_6$[2] and $AgPb_mSbTe_{2+m}$,[3] showing satisfactory thermoelectric properties were recently reported.

Many multinary main-group metal chalcogenides were discovered during the past decade. Among these materials, most are sulfides that contain heavy elements (Sb, Bi, Sn, Pb, etc.), and their structures exhibit complicated structural types because of stereochemically active lone pairs of electrons for those cations that distort the cation environment.[4] Significantly distorted cation environments are commonly observed in ternary Pb-(Sb, Bi)-(S, Se) systems such as $Pb_3Bi_2S_6$,[5] $Pb_6Bi_2S_9$,[6] $PbBi_2S_4$,[7] $Pb_2Bi_2S_5$,[8] $Pb_{46}Bi_{54}S_{127}$,[9] $PbBi_4S_7$,[10] $Pb_9Sb_9S_{22}$,[11] $Pb_5Sb_8S_{17}$,[12] $Pb_3Sb_8S_{15}$,[13] $Pb_7Sb_8S_{19}$,[14] $Pb_{1.6}Sb_{3.4}S_7$,[15] $Pb_5Sb_4S_{11}$,[16] $Pb_4Sb_6S_{13}$,[17] $Pb_2Sb_2S_5$,[18] $Pb_5Sb_6S_{14}$,[19] $Pb_{3.58}Sb_{4.42}Se_{10}$,[20] $PbSb_2Se_4$,[21] $Pb_6Sb_6Se_{17}$,[22] $Pb_4Sb_6Se_{13}$,[23] and so forth. We have investigated the effect of indium or transition metals on the structures

*To whom correspondence should be addressed. E-mail: chishen@mail.nctu.edu.tw.

(1) Rowe, D. M. *CRC Handbook of Thermoelectrics*; Boca Raton, FL: CRC Press, 1995.
(2) Chung, D.-Y.; Hogan, T.; Brazis, P.; Rocci-Lane, M.; Kannewurf, C.; Bastea, M.; Uher, C.; Kanatzidis, M. G. *Science* **2000**, *287*, 1024–1027.
(3) Hsu, K. F.; Loo, S.; Guo, F.; Chen, W.; Dyck, J. S.; Uher, C.; Hogan, T.; Polychroniadis, E. K.; Kanatzidis, M. G. *Science* **2004**, *303*, 818–821.
(4) Kanatzidis, M. G.; McCarthy, T. J.; Tanzer, T. A.; Chen, L.-H.; Iordanidis, L. *Chem. Mater.* **1996**, *8*, 1465–1474.
(5) Berlepsch, P.; Armbruster, T.; Makovicky, E.; Hejny, C.; Topa, D.; Graeser, S. *Can. Mineral.* **2001**, *39*, 1653–1663.
(6) Takéuchi, Y.; Takagi, J. *Proc. Jpn. Acad.* **1974**, *50*, 76–79.
(7) Olsen, L. A.; Balic-Žunic, T.; Makovicky, E.; Ullrich, A.; Miletich, R. *Phys. Chem. Miner.* **2007**, *34*, 467–475.
(8) Weitz, G.; Hellner, E. *Z. Kristallogr.* **1960**, *113*, 385–402.
(9) Matzat, E. *Acta Crystallogr., Sect. B: Struct. Sci.* **1979**, *35*, 133–136.
(10) Takéuchi, Y.; Takagi, J.; Yamanaka, T. *Proc. Jpn Acad.* **1974**, *50*, 317–321.
(11) Born, L.; Hellner, E. *Am. Mineral.* **1960**, *45*, 1266–1271.
(12) Seung-Am, C.; Wuensch, B. J. *Nature* **1970**, *225*, 444–445.
(13) Nuffield, E. W. *Acta Crystallogr., Sect. B: Struct. Sci.* **1975**, *31*, 151–157.
(14) Edenharter, A. *Z. Kristallogr.* **1980**, *151*, 193–202.
(15) Lebas, G.; le Bihan, M. T. *Bull. Soc. Fr. Mineral. Cristallogr.* **1976**, *99*, 351–360.
(16) Skowron, A.; Brown, I. D. *Acta Crystallogr., Sect. C: Cryst. Struct. Commun.* **1990**, *46*, 531–534.
(17) Skowron, A.; Brown, I. D. *Acta Crystallogr., Sect. C: Cryst. Struct. Commun.* **1990**, *46*, 527–531.
(18) Skowron, A.; Brown, I. D. *Acta Crystallogr., Sect. C: Cryst. Struct. Commun.* **1990**, *46*, 534–536.
(19) Skowron, A.; Brown, I. D.; Tilley, R. J. D. *J. Solid State Chem.* **1992**, *97*, 199–211.
(20) Skowron, A.; Brown, I. D. *Acta Crystallogr., Sect. C: Cryst. Struct. Commun.* **1990**, *46*, 2287–2291.
(21) Skowron, A.; Boswell, F. W.; Corbett, J. M.; Taylor, N. J. *J. Solid State Chem.* **1994**, *112*, 251–254.
(22) Emirdag-Eanes, M.; Kolis, J. W. *Z. Anorg. Allg. Chem.* **2002**, *628*, 10–11.
(23) Derakhshan, S.; Assoud, A.; Taylor, N. J.; Kleinke, H. *Intermetallics* **2006**, *14*, 198–207.

Published on Web 06/17/2009

and properties of quaternary chalcogenides containing heavy main-group elements Sb, Bi, Sn, and Pb.[24] Before this work the reported phases were quaternary sulfides $Pb_{1.6}In_8Bi_4S_{19}$,[25] $Pb_4In_3Bi_7S_{18}$,[26] and $Pb_4In_2Bi_4S_{13}$.[27] No quaternary phase has been reported in the In−Pb−M−Se (M = Sb, Bi) system.

The substitution of indium for a bismuth cation might cause a considerable alteration of the crystal structure and electronic properties because of fewer valence electrons and a smaller atomic radius. Our exploratory work in the quaternary Pb−In−M−Se (M = Sb, Bi) system yielded several new quaternary phases with general formula $Pb_4In_xM_{6-x}Se_{13}$ (M = Bi, $x = 2.1-2.8$; Sb, $x = 2$). The quaternary $Pb_4In_xBi_{6-x}Se_{13}$ shows a measurable phase width, and varying the In/Bi ratio produces significant variation of the physical and electronic properties. Here we report the synthesis, structural characterization, measurements of physical properties, and calculations of electronic structure of $Pb_4In_xM_{6-x}Se_{13}$ (M = Bi, $x = 2.1-2.8$; Sb, $x = 2$).

Experiments

Synthesis. All operations on compounds were performed in a glovebox with a dry nitrogen atmosphere. Chemicals were used as obtained (from Alfa Aesar): Sb, 99.5%, powder; Bi, 99.5%, powder; In, 99.99%, powder; Pb, 99.9%, powder; Se, 99.95%, powder. The total masses of samples (all elements combined) were about 0.5 g. All reactants in evacuated fused-silica tubes were placed in resistance furnaces with controlled temperature.

$Pb_4In_{2.1}Bi_{3.9}Se_{13}$ was initially observed as a product from a reaction with a molar ratio Pb/In/Bi/Se = 2:1:3:8. The reaction mixture was heated from 300 to 1023 K over 8 h; the latter temperature was maintained for 16 h before natural cooling to about 300 K. Observed under an optical microscope, the product contained a molten part and small particles with a metallic luster. On the basis of measurements of powder X-ray diffraction, the product of the "$Pb_2InBi_3Se_8$" reaction is a mixture of $Pb_5Bi_6Se_{14}$,[28] $Pb_2Bi_2Se_5$,[29] and an unknown phase. After the crystal structure and composition were confirmed as $Pb_4In_{2.1}Bi_{3.9}Se_{13}$, reactions with varied proportions of In in $Pb_4In_xBi_{6-x}Se_{13}$ ($x = 0-6.0$) were tested to probe the possible phase width under heating conditions the same as specified above. The products of each reaction revealed silvery, brittle ingots that were sensitive to neither air nor moisture. On the basis of powder X-ray diffraction and energy-dispersive spectra (EDX), a pure phase of $Pb_4In_xBi_{6-x}Se_{13}$ ($x = 2.5-3.0$) was synthesized, but the single-crystalline sample yielded a refined formula $Pb_4In_{2.1}Bi_{3.9}Se_{13}$ ($x = 2.1$, from the "$Pb_2InBi_3Se_8$" reaction) and $Pb_4In_{2.8}Bi_{3.2}Se_{13}$ ($x = 2.8$, from a "$Pb_4In_3Bi_3Se_{13}$" reaction). The experimental X-ray powder-diffraction patterns agreed satisfactorily with patterns simulated based on single-crystal data, confirming the phase purity of the products as synthesized (Supporting Information, Figure S1). For reactions with x in regions $0 < x < 2.5$ and $3 < x < 6.0$, the products contain mixtures of $Pb_4In_xBi_{6-x}Se_{13}$, $Pb_5Bi_6Se_{14}$, $Pb_{7.12}In_{18.88}Se_{34}$,[30] Bi_2Se_3,[31] and In_2Se_3.[32] The results of powder and single-crystal X-ray measurements show that the unit cell and volume varied gradually with increasing In content. Attempts to synthesize ternary phases of "$Pb_4Bi_6Se_{13}$" and "$Pb_4In_6Se_{13}$" failed; the products comprised known phases $Pb_5Bi_6Se_{14}$ and $Pb_{7.12}In_{18.88}Se_{34}$, respectively. Other possible variations in the $M_4In_xM'_{6-x}X_{13}$ (M = Ge, Sn, and Pb; M′ = Sb, Bi; X = S, Se, and Te; $x = 2$, 3) were tested; only the product from the reaction of "$Pb_4In_2Sb_4Se_{13}$" contained a mixture of $Pb_4In_2Sb_4Se_{13}$, $PbSb_2Se_4$, and an unknown phase.

Single-Crystal X-ray Diffraction (XRD). Single crystals of $Pb_4In_{2.1}Bi_{3.9}Se_{13}$, $Pb_4In_{2.8}Bi_{3.2}Se_{13}$, and $Pb_4In_2Sb_4Se_{13}$ were mounted on glass fibers with epoxy glue; intensity data were collected on a diffractometer (Bruker APEX CCD) with graphite-monochromated Mo-K_α radiation ($\lambda = 0.71073$ Å) at 298(2) K. The distance from crystal to detector was 5.038 cm. Data were collected on scanning $\omega = 0.3°$ in groups of 600, 600, 435, and 435 frames each at φ settings 0°, 90°, 180°, and 270°. The duration of exposure was 30, 20, and 30 s/frame for $Pb_4In_{2.1}Bi_{3.9}Se_{13}$, $Pb_4In_{2.8}Bi_{3.2}Se_{13}$, and $Pb_4In_2Sb_4Se_{13}$, respectively. Values of theta varied between 1.18° and 28.56°. Diffraction signals obtained from all frames of reciprocal space images were used to determine the parameters of the unit cell. The data were integrated (Siemens SAINT program) and corrected for Lorentz and polarization effects.[33] Absorption corrections were based on a function fitted to an empirical transmission surface as sampled with multiple equivalent measurements of numerous reflections using SADABS.[34] The structural model was obtained with direct methods and refined with full-matrix least-squares refinement based on F^2 using the SHELXTL package.[35]

$Pb_4In_{2.1}Bi_{3.9}Se_{13}$ and $Pb_4In_{2.8}Bi_{3.2}Se_{13}$ as synthesized revealed a primitive orthorhombic unit cell; systematic absences indicated *Pbam* and *Pba*2 as the possible space groups. The centrosymmetric space group *Pbam* was chosen at the end of the refinement for smaller values of reliability factors. Using direct methods, a structural model was built with 11 unique sites for metal atoms (In, Pb, and Bi) and 13 unique sites for Se atoms. The initial model of the crystal structure was based on an isostructural compound $Pb_4In_2Bi_4S_{13}$ with fully occupied sites for metal and Se atoms, but structural refinements displayed unreasonable isotropic displacement parameters (U_{iso}) of the M5−M10 sites (identical to Bi and In fully occupied sites in the structure of $Pb_4In_2Bi_4S_{13}$), indicative of positions with partial or mixed occupancy by In and Bi cations. Subsequent refinements were performed on varying the distributions of In and Bi in the M5−M10 sites, and a charge-balanced model was eventually constructed as $(Pb^{2+})_4(In^{3+})_x(Bi^{3+})_{6-x}(Se^{2-})_{13}$ ($x = 2.1$, 2.8).

For the X-ray diffraction of $Pb_4In_2Sb_4Se_{13}$, a single crystal of acceptable quality was difficult to obtain because the sample was isolated from mixtures of $Pb_4In_2Sb_4Se_{13}$, $PbSb_2Se_4$, and an unknown phase. Several crystals from the crushed product were used for single-crystal X-ray diffraction, but the diffraction features were indexed to an orthorhombic lattice with large standard deviations of the lattice parameters, which indicate poor quality of these crystals. The diffraction pattern from the best crystal showed that several reflections in the region of high angle exhibit split peaks, which might be contributed by a closely aligned crystal. Attempt to separate these split signals for structural refinement failed. The structural refinements for $Pb_4In_2Sb_4Se_{13}$ were similar to $Pb_4In_xBi_{6-x}Se_{13}$ ($x = 2.1$, 2.8), but were performed with a fully occupied model because of the

(24) Wang, K.-C.; Lee, C.-S. *Inorg. Chem.* **2006**, *45*, 1415–1417.
(25) Kraemer, V. *Acta Crystallogr., Sect. C: Cryst. Struct. Commun.* **1983**, *39*, 1328–1329.
(26) Kraemer, V.; Reis, I. *Acta Crystallogr., Sect. C: Cryst. Struct. Commun.* **1986**, *42*, 249–251.
(27) Kraemer, V. *Acta Crystallogr., Sect. C: Cryst. Struct. Commun.* **1986**, *42*, 1089–1091.
(28) Zhang, Y. G.; Wilkinson, A. P.; Lee, P. L.; Shastri, S. D.; Shu, D. M.; Chung, D. Y.; Kanatzidis, M. G. *J. Appl. Crystallogr.* **2005**, *38*, 433–441.
(29) Agaev, K. A.; Talybov, A. G.; Semiletov, S. A. *Kristallografiya* **1966**, *11*, 736–740.
(30) Eddike, D.; Ramdani, A.; Brun, G.; Liautard, B.; Tedenac, J. C.; Tillard, M.; Belin, C. *Eur. J. Solid State Inorg. Chem.* **1997**, *34*, 309–316.
(31) Nakajima, S. *J. Phys. Chem. Solids* **1963**, *24*, 479–485.
(32) Osamura, K.; Murakami, Y.; Tomiie, Y. *J. Phys. Soc. Jpn.* **1966**, *21*, 1848–1848.
(33) *SAINT*, Version 6.22; Siemens Analytical X-ray Instruments Inc.: Madison, WI, 2001.
(34) *SADABS, Bruker/Siemens area detector absorption and other corrections*, V2.03; Bruker Analytical X-ray Systems, Inc.: Madison, WI, 2001.
(35) *SHELXTL*, Version 6.10 Reference Manual; Siemens Analytical X-Ray Systems, Inc.: Madison, WI, 2000.

Table 1. Crystal Data and Conditions of Data Collection for $Pb_4In_{2.1}Bi_{3.9}Se_{13}$, $Pb_4In_{2.8}Bi_{3.2}Se_{13}$, and $Pb_4In_2Sb_4Se_{13}$

refined composition	$Pb_4In_{2.1}Bi_{3.9}Se_{13}$	$Pb_4In_{2.8}Bi_{3.2}Se_{13}$	$Pb_4In_2Sb_4Se_{13}$
formula mass/g mol^{-1}	2911.42	2845.51	2571.96
instrument; temperature	Smart CCD; 298(2)		
wavelength	0.71073 Å		
crystal system	orthorhombic		
space group, Z	*Pbam* (55), 4		
a/Å	22.273(5)	22.065(4)	21.722(4)
b /Å	27.488(6)	27.420(6)	27.140(5)
c /Å	4.1418(8)	4.1272(8)	4.0621(8)
V/Å^3	2535.8(9)	2497.1(9)	2394.7(8)
θ_{min}, θ_{max}/deg	1.18, 28.34	1.18, 28.35	1.20,28.56
independent(R_{int}), observed reflections	3603(0.0586), 29610	3555(0.0511), 28899	3471(0.0969), 27207
$d_{calcd.}$/g cm^{-3}	7.626	7.569	7.136
absorption coefficient/mm^{-1}	73.930	70.796	54.082
reflections collected	29610	28899	27207
refinement method	full-matrix least-squares on F^2		
goodness of fit on F^2	1.168	1.141	1.201
R_1, wR_2 (all data)[a]	0.0398, 0.0700	0.0447, 0.0918	0.0864, 0.1339
R_1, wR_2 ($I > 2\sigma(I)$)	0.0315, 0.0676	0.0365, 0.0877	0.0576, 0.1247

[a] $R1 = \sum||F_o| - |F_c||/\sum|F_o|$, $wR_2 = \{\sum w(F_o^2 - F_c^2)^2/\sum w(F_o^2)^2\}^{1/2}$.

similar atomic numbers of In and Sb. The M1−M4, M5−M8, and M9−M11 sites are assigned as fully occupied by Pb, Sb, and In atoms, respectively. During the latter stages of refinement, one large peak (~7 e/Å^3) appeared in the map of electron density in positions near sites Pb2, which might reflect a contribution of twin components. Those peaks were made to refine as partially occupied Pb atoms, but refined formulas were not charge-balanced to justify that refinement. These signals were hence excluded as atoms in the final model because of the uncertainty regarding these features. Assuming In^{3+}, Pb^{2+}, Sb^{3+}, and Se^{2-}, a charge-balanced formula $(Pb^{2+})_4(In^{3+})_2(Sb^{3+})_4(Se^{2-})_{13}$ was constructed.

We tried both on single and twinned crystal approaches for crystal data $Pb_4In_2Sb_4Se_{13}$ and $Pb_4In_{2.8}Bi_{3.2}Se_{13}$ that contain high residual electron densities near the Pb2 site. Refining a model with positional disorder of Pb atom (Pb2a and Pb2b) for both crystal data slightly improved the R-factors and the residual electron density reduced to ~4 e Å^{-3}. However, the refinement based on split Pb2 site was unstable, and the standard deviation for atomic displacement and atomic coordinate parameters are 5−10 times larger than other atomic sites. The residual electron density reduced significantly to ~ 3 e/Å^{-3} when the high angle data were excluded from the refinement (2 theta > 40 degree). The results suggest that these crystal data contain contributions that come from a twin or a small crystal attached to it. However, attempts to use the twin index and data collection/absorption correction programs (GEMINI. Version 1.02,[36] HKL5 format) did not improve the results. We think the structure model for both samples are correct since they are isostructural with $Pb_4In_{2.1}Bi_{3.9}Se_{13}$.

Crystallographic data and selected bond distances for $Pb_4In_{2.1}Bi_{3.9}Se_{13}$, $Pb_4In_{2.8}Bi_{3.2}Se_{13}$, and $Pb_4In_2Sb_4Se_{13}$ are given in Tables 1−4 and Supporting Information,Tables S1−S3. Further details of the crystal-structure investigation are obtainable from Fachinformationszentrum Karlsruhe, Eggenstein-Leopoldshafen, Germany (Fax: +49 7247 808 666; E-mail: crysdata@fiz.karlsruhe.de) on quoting the depository number CSD- 420647, 420648, and 420649.

Characterization. X-ray powder-diffraction data of the products were measured on a powder diffractometer of Bragg−Brentano-type (Bruker D8 Advance, operated at 40 kV and 40 mA, Cu K_α, λ = 1.5418 Å). For phase identification, XRD data were collected in a 2θ range from 5° to 60° with a step interval 0.05° and 1 s/step counting time. The lattice parameters were calculated with least-squares fitting using the CELREF program.[37] The bond valence calculations were performed using Bond Valence theory.[38] Diffuse reflectance measurements were performed near 300 K with a UV−visible spectrophotometer (Jasco V-570); an integrating sphere was used to measure diffuse reflectance spectra over a range 200−2000 nm. Samples as ground powder were pressed onto a thin glass-slide holder; a $BaSO_4$ plate served as reference. Energy-dispersive spectra

Table 2. Atomic Coordinates, Site Occupancies, and Isotropic Displacement Parameters (U_{eq} /10^{-3} Å^2) for $Pb_4In_{2.1}Bi_{3.9}Se_{13}$

atom	site	x	y	z	U_{eq}[a]	site occ.	
M1	4h	0.6264(1)	0.7500(1)	0.5	36(1)	Pb	
M2	4h	0.1843(1)	0.0701(1)	0.5	38(1)	Pb	
M3	4h	0.1675(1)	0.2245(1)	0.5	37(1)	Pb	
M4	4h	0.4678(1)	0.8458(1)	0.5	32(1)	Pb	
M5	4h	0.8850(1)	0.0847(1)	0.5	18(1)	Bi	0.980(5)
						In	0.020
M6	4h	0.6545(1)	0.0239(1)	0.5	18(1)	Bi	0.949(5)
						In	0.051
M7	4g	0.6434(1)	0.8910(1)	0	17(1)	Bi	0.914(5)
						In	0.086
M8	4g	0.0224(1)	0.1567(1)	0	17(1)	Bi	0.802(5)
						In	0.198
M9	2c	0.5	0	0	16(1)	Bi	0.346(7)
						In	0.654
M10	2a	0	0	0	18(1)	Bi	0.168(7)
						In	0.832
M11	4g	0.7255(1)	0.1610(1)	0	19(1)	In	
Se1	4h	0.0258(1)	0.2234(1)	0.5	16(1)		
Se2	4h	0.7462(1)	0.1059(1)	0.5	15(1)		
Se3	4g	0.5606(1)	0.8134(1)	0	16(1)		
Se4	4g	0.8805(1)	0.0077(1)	0	20(1)		
Se5	4g	0.5824(1)	0.0736(1)	0	21(1)		
Se6	4h	0.5628(1)	0.9479(1)	0.5	16(1)		
Se7	4g	0.1489(1)	0.1441(1)	0	18(1)		
Se8	4g	0.3806(1)	0.7998(1)	0	17(1)		
Se9	4h	0.0112(1)	0.0713(1)	0.5	17(1)		
Se10	4g	0.7256(1)	0.9765(1)	0	21(1)		
Se11	4g	0.8932(1)	0.1591(1)	0	20(1)		
Se12	4h	0.7097(1)	0.8507(1)	0.5	17(1)		
Se13	4g	0.7275(1)	0.7464(1)	0	17(1)		

[a] U_{eq} is defined as one-third of the trace of the orthogonalized U_{ij} tensor.

(36) *GEMINI*, Version 1.02; Siemens Analytical X-ray Instruments Inc.: Madison, WI., 2003.

(37) Laugier, J.; Bochu, B., Celref, http://www.inpg.fr/LMGP; Laboratoire des Materiaux et du Génie Physique de l'Ecole Supérieure de Physique de Grenoble.

(38) Altermatt, U. D.; Brown, I. D. *Acta Crystallogr., Sect. A: Found. Crystallogr*. **1987**, *43*, 125–130.

Table 3. Atomic Coordinates, Site Occupancies, and Isotropic Displacement Parameters ($U_{eq}/10^{-3}$ Å^2) for $Pb_4In_{2.8}Bi_{3.2}Se_{13}$

atom	site	*x*	*y*	*z*	U_{eq}[a]	site occ.	
M1	4h	0.6260(1)	0.7505(1)	0.5	37(1)	Pb	
M2	4h	0.1819(1)	0.0712(1)	0.5	37(1)	Pb	
M3	4h	0.1663(1)	0.2262(1)	0.5	35(1)	Pb	
M4	4h	0.4688(1)	0.8467(1)	0.5	33(1)	Pb	
M5	4h	0.8862(1)	0.0850(1)	0.5	19(1)	Bi	0.842(6)
						In	0.158
M6	4h	0.6546(1)	0.0231(1)	0.5	18(1)	Bi	0.876(6)
						In	0.124
M7	4g	0.6447(1)	0.8913(1)	0	19(1)	Bi	0.730(6)
						In	0.270
M8	4g	0.0225(1)	0.1576(1)	0	21(1)	Bi	0.564(6)
						In	0.436
M9	2c	0.5	0	0	19(1)	Bi	0.210(8)
						In	0.790
M10	2a	0	0	0	22(1)	Bi	0.177(8)
						In	0.823
M11	4g	0.7274(1)	0.1602(1)	0	21(1)	In	
Se1	4h	0.0256(1)	0.2235(1)	0.5	17(1)		
Se2	4h	0.7481(1)	0.1048(1)	0.5	19(1)		
Se3	4g	0.5614(1)	0.8151(1)	0	20(1)		
Se4	4g	0.8801(1)	0.0094(1)	0	26(1)		
Se5	4g	0.5818(1)	0.0721(1)	0	22(1)		
Se6	4h	0.5631(1)	0.9479(1)	0.5	19(1)		
Se7	4g	0.1464(1)	0.1442(1)	0	21(1)		
Se8	4g	0.3799(1)	0.8014(1)	0	19(1)		
Se9	4h	0.0133(1)	0.0719(1)	0.5	21(1)		
Se10	4g	0.7252(1)	0.9757(1)	0	27(1)		
Se11	4g	0.8958(1)	0.1585(1)	0	27(1)		
Se12	4h	0.7107(1)	0.8513(1)	0.5	18(1)		
Se13	4g	0.7267(1)	0.7459(1)	0	19(1)		

[a] U_{eq} is defined as one-third of the trace of the orthogonalized U_{ij} tensor.

Table 4. Atomic Coordinates, Site Occupancies, and Isotropic Displacement Parameters ($U_{eq}/10^{-3}$ Å^2) for $Pb_4In_2Sb_4Se_{13}$

atom	site	*x*	*y*	*z*	U_{eq}[a]
Pb1	4h	0.6232(1)	0.7497(1)	0.5	39(1)
Pb2	4h	0.1779(1)	0.0723(1)	0.5	36(1)
Pb3	4h	0.1685(1)	0.2286(1)	0.5	34(1)
Pb4	4h	0.4686(1)	0.8497(1)	0.5	32(1)
Sb5	4h	0.8888(1)	0.0840(1)	0.5	22(1)
Sb6	4h	0.6541(1)	0.0205(1)	0.5	19(1)
Sb7	4g	0.6470(1)	0.8909(1)	0	27(1)
Sb8	4g	0.0222(1)	0.1588(1)	0	30(1)
In9	2c	0.5	0	0	23(1)
In10	2a	0	0	0	21(1)
In11	4g	0.7300(1)	0.1556(1)	0	26(1)
Se1	4h	0.0246(1)	0.2225(1)	0.5	21(1)
Se2	4h	0.7515(1)	0.0981(1)	0.5	23(1)
Se3	4g	0.5629(1)	0.8192(1)	0	22(1)
Se4	4g	0.8780(1)	0.0152(1)	0	22(1)
Se5	4g	0.5876(1)	0.0683(1)	0	26(1)
Se6	4h	0.5632(1)	0.9478(1)	0.5	23(1)
Se7	4g	0.1430(1)	0.1437(1)	0	21(1)
Se8	4g	0.3785(1)	0.8042(1)	0	21(1)
Se9	4h	0.0152(1)	0.0709(1)	0.5	23(1)
Se10	4g	0.7187(1)	0.9749(1)	0	28(1)
Se11	4g	0.8975(1)	0.1533(1)	0	28(1)
Se12	4h	0.7110(1)	0.8531(1)	0.5	24(1)
Se13	4g	0.7254(1)	0.7431(1)	0	21(1)

[a] U_{eq} is defined as one-third of the trace of the orthogonalized U_{ij} tensor.

(SEM/EDX, Hitachi S-4700I High-Resolution Scanning Electron Microscope) were recorded on crystalline samples of rod and needle shapes. The elements In, Pb/Bi, and Se were present in several crystals. The Pb/Bi ratio was indeterminate because of severe overlap of signals due to Pb and Bi in the SEM/EDX system. Measurements of differential scanning calorimetry (DSC) and thermogravimetry (TG) were performed with a thermal analyzer (NETZSCH STA 409PC) with a powder sample (approximately 40 mg) placed in an alumina crucible; Al_2O_3 powder served as a reference sample. The sample was heated to 1673 at 10 K/min under a constant flow of N_2.

Calculation of the Electronic Structure. Band calculations with tight-binding linear muffin-tin orbitals (LMTO) using an atomic sphere approximation (ASA) were undertaken to provide information about the electronic structures.[39−43] Density-functional theory was employed with the local-density approximation (LDA) for the exchange-correlation energy. Four models were constructed with space group *Pbam* to simulate the observed crystal structures containing sites of mixed occupancy and the phase width. Integration in *k* space was performed with an improved tetrahedron method on grids $8 \times 8 \times 24$ of unique *k* points in the first Brillouin zone. We analyzed the electronic structure by extracting information from the band structure, densities of states (DOS), and crystal-orbital Hamiltonian population curves (COHP).[44]

Physical Property Measurements. We measured Seebeck coefficients on a cold-pressed bar ($1 \times 1 \times 5$ mm^3) with a commercial apparatus for thermopower measurement (MMR Technologies) in the temperature range 300−600 K under a dynamic vacuum ($\sim 10^{-2}$ Torr). Constantan served as an internal standard, and electric contacts were created with silver conductive paint. Measurements of direct current (DC) conductivity were performed with a standard four-probe method under vacuum ($\sim 10^{-2}$ Torr) in the temperature range 30−300 K. To decrease an effect of grain boundaries of crystalline powder on the conductivity measurements, each cold-pressed sample was annealed at 773 K for 72 h before each measurement.

Results and Discussion

Description of the Structure. $Pb_4In_{2.1}Bi_{3.9}Se_{13}$, $Pb_4In_{2.8}Bi_{3.2}Se_{13}$, and $Pb_4In_2Sb_4Se_{13}$ crystallize in an isostructural form, $Pb_4In_2Bi_4S_{13}$, with orthorhombic space group *Pbam* (No. 55) and four formula units per unit cell. A section of the $Pb_4In_{2.1}Bi_{3.9}Se_{13}$ structure is shown in Figure 1. The structure features a three-dimensional framework comprising *Z*-shaped ribbon units and corner-sharing infinite one-dimensional $[InSe_4]_\infty$ chains running parallel to the *c*-axis; these layers are connected with Pb atoms to form three-dimensional structures. The structure contains 24 crystallographically inequivalent sites, 11 for cations (In^{3+}, Pb^{2+}, Sb^{3+}, and Bi^{3+}) and 13 for anions (Se^{2-}). The coordination environment of metal sites is grouped into three types. (1) Site M1−M4 (100% Pb) has a bicapped trigonal prism coordination with Pb−Se distances in a range 3.01−3.53 Å. A similar coordination of lead ion was observed in other multinary lead chalcogenides such as $Y_6Pb_2Se_{11}$.[45] (2) Sites M5−M10 have mixed occupancy by Bi and In atoms. The coordination polyhedra around M5−M8 sites (B*i* > 50%) are distorted octahedra with three short M−Se

(39) Andersen, O. K. *Phys. Rev. B* **1975**, *12*, 3060.
(40) Skriver, H. L. *The LMTO Method*; Springer: Berlin, 1984.
(41) van Barth, U.; Hedin, L. *J. Phys. C* **1971**, *4*, 2064.
(42) Blöhl, P. E.; Jepsen, O.; Andersen, O. K. *Phys. Rev. B: Condens. Matter* **1994**, *49*, 16223–33.
(43) Jepsen, O.; Andersen, O. K. *Z. Phys.* **1995**, *97*, 25.
(44) Dronskowski, R.; Blöhl, P. E. *J. Phys. Chem.* **1993**, *97*, 8617.
(45) Gulay, L. D.; Shemet, V. Y.; Stepien-Damm, J.; Pietraszko, A.; Olekseyuk, I. D. *J. Alloys Compd.* **2005**, *403*, 206–210.

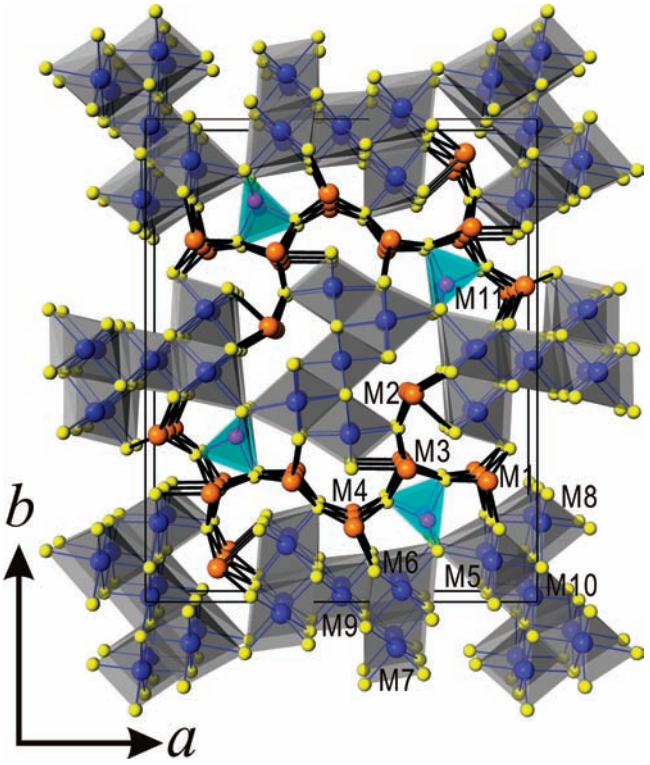

Figure 1. Crystal structure of $Pb_4In_{2.1}Bi_{3.9}Se_{13}$ in a projection along the crystallographic *c*-axis [001], showing Pb atoms in bicapped trigonal prism sites (M1−M4, orange), *Z*-shaped ribbons (M5−M10, gray octahedra), and $[InSe_4]_\infty$ chains (M11, light blue).

bonds (2.76−2.93 Å) opposite three longer ones (2.87−3.16 Å) attributed to the $6s^2$ lone-pair effect of the Bi^{3+} cation, as observed in similar Bi−Se contacts for known chalcogenides with Bi as a constituent element, such as Bi_2Se_3. M9 and M10 sites are hexacoordinate in a less distorted octahedron with M−Se distances in a range 2.66−2.89 Å and In occupancy > 50%, comparable to the In−Se distance in $Pb_{7.12}In_{18.88}Se_{34}$. These octahedral clusters build to form one-dimensional, *Z*-shaped ribbons with edge or corner sharing. (3) Site M11 is fully In, surrounded by four Se atoms forming a distorted tetrahedron with In−Se distances in a range 2.56−2.61 Å. These tetrahedral units form a chain along the *c* direction on sharing two vertices. For the In-rich phase $Pb_4In_{2.8}Bi_{3.2}Se_{13}$, the In atoms fill the M5−M9 sites; the site compositions of sites M1−M4 and M10−M11 remain the same as for $Pb_4In_{2.1}Bi_{3.9}Se_{13}$, which indicates that the distorted environments of M1−M4 sites are not favored for In atoms. The average bond lengths of M5−Se, M6−Se, M7−Se, M8−Se, and M9−Se decrease with increasing In concentration of the compound. This trend is identical to that of the ionic radius of In^{3+} (0.94 Å) smaller than Bi^{3+} (1.17 Å).[46] Supporting Information, Figure S2 shows the refined lattice parameters for $Pb_4In_xBi_{6-x}Se_{13}$ ($x = 2.0-3.0$). In general, the refined lattice parameters were gradually decreased as the composition of In increased. The cell volume decreased slightly with increasing In content in $Pb_4In_xBi_{6-x}Se_{13}$ for $2.5 \le x \le 3.0$, which might be due to small ionic radius of In^{3+}. The cell volumes obtained for $Pb_4In_xBi_{6-x}Se_{13}$ prepared with $2.0 < x < 2.5$ were found to be constant, indicative of a fixed composition of the major product. The lattice parameters for samples with $x < 2.0$ and $3.0 < x < 6.0$ could not be indexed because of severely overlapped powder patterns with the major phase $Pb_5Bi_6Se_{14}$ and $Pb_{7.12}In_{18.88}Se_{34}$. For the Sb-substituted phase $Pb_4In_2Sb_4Se_{13}$, a significantly decreased volume of the unit cell was observed because the ionic radius of Sb^{3+} (0.90 Å)[46] is smaller than that of Bi^{3+} (1.17 Å). The distorted environments of sites M1−M4 are assigned to Pb for its localized $6s^2$ electrons. Sites Sb5−Sb8 are assigned to Sb, similar to the Bi rich sites in the structure of $Pb_4In_xBi_{6-x}Se_{13}$. The interatomic distances of Sb−Se contacts are in a range 2.65−3.01 Å. Sites In9−M11 are assigned fully to In with slightly distorted octahedral or tetrahedral environments. Compared with $Pb_4In_xM_{6-x}Se_{13}$ and Sb-substituted phase $Pb_4In_2Sb_4Se_{13}$, Pb atoms and Bi atoms are distinguishable according to their coordination environments in those structures. The Pb $6s^2$ lone-pair elections favor localization to form a distorted environment whereas Bi prefers to have an octahedral environment. Bond valence sum calculations indicate that all atoms in the M1−M4 sites have formal oxidation numbers within 2.05−2.31 with parameters of Pb^{2+}; the results are in satisfactory agreement with formal oxidation states of Pb^{2+}. Calculations using parameters of In^{3+}, Bi^{3+} show unreasonable oxidation states for In^{3+} (1.17−1.33) and Bi^{3+} (2.09−2.31), respectively.

Electronic Structure. To understand the quaternary phases as synthesized, containing Bi/In sites of mixed occupancy, and the phase width, we constructed four models with varied assignment of metal sites (Supporting Information,Tables S4) to Pb (M1−M4), Bi (M5−M7), and Bi/In (M8−M11) and performed calculations of the electronic structure. These models generate hypothetical formulas $Pb_4Bi_6Se_{13}$(**1**), $Pb_4(In_1Bi_5)Se_{13}$(**2**), $Pb_4(In_2Bi_4)Se_{13}$(**3**), and $Pb_4(In_3Bi_3)Se_{13}$(**4**). The electronic band structures were calculated with a tight-binding method using the LMTO program. Curves for the total and partial densities of states (DOS, PDOS) for these models appear in Figure 2. The calculated band structures show indirect band gaps 0.51, 0.83, 0.89, and 0.60 eV for **1**, **2**, **3**, and **4**, respectively, indicative of a semiconducting property. Model **3** and **4** are near the crystal data of $Pb_4In_{2.1}Bi_{3.9}Se_{13}$ and $Pb_4In_{2.8}Bi_{3.2}Se_{13}$ as refined, respectively. The DOS curves indicate that contributions near the Fermi level (E_F) are composed of mostly Pb(6p) and Bi(6p) states mixed with In(6s) states in a small proportion. The large feature between −5 eV and the Fermi level is dominated by Se (3p) and Bi/Pb (6p) states. The sharp features at −10 and −8 eV are from the filled $6s^2$ state of Bi and Pb atoms, which might be due to the inert-pair effect in heavy main-group elements. As the proportion of In increases, the valence electron concentration per formula (vec) decreases, which is evidence that the PDOS of Bi ($6s^2$) from sites M8−M11 decreases when these sites are gradually replaced by In atoms. The DOS curves show that the valence bands are filled for all models.

Curves for the crystal-orbital Hamiltonian population (COHP) for models with varied assignments of In or Bi at sites M8−M11 appear in Figure 3. These results show

(46) Shannon, R. D. *Acta Crystallogr., Sect. A: Cryst. Phys., Diffr., Theor. Gen. Cryst.* **1976**, *32*, 751–767.

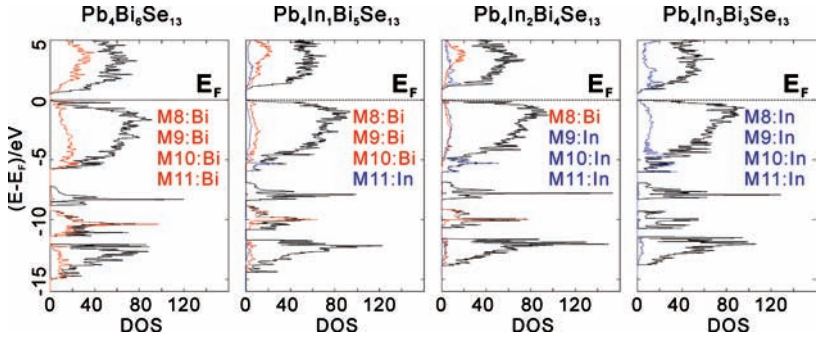

Figure 2. Calculated curves of total DOS (black line) and PDOS (M8−M11 sites, red line for Bi and blue line for In) for $Pb_4Bi_6Se_{13}$(**1**), $Pb_4(In_1Bi_5)Se_{13}$(**2**), $Pb_4(In_2Bi_4)Se_{13}$(**3**), and $Pb_4(In_3Bi_3)Se_{13}$(**4**). The horizontal line denotes the Fermi energy (E_F).

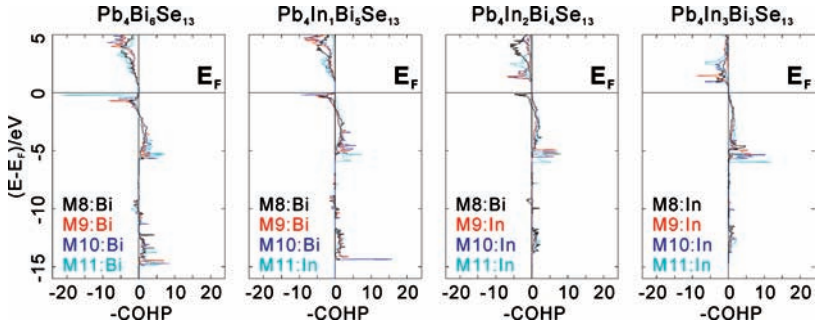

Figure 3. Curves of crystal orbital Hamiltonian populations (COHP) for M−Se contacts (M8−Se, black; M9−Se, red; M10−Se, blue; and M11−Se, light blue) from models **1**−**4**. The horizontal line denotes the Fermi energy (E_F).

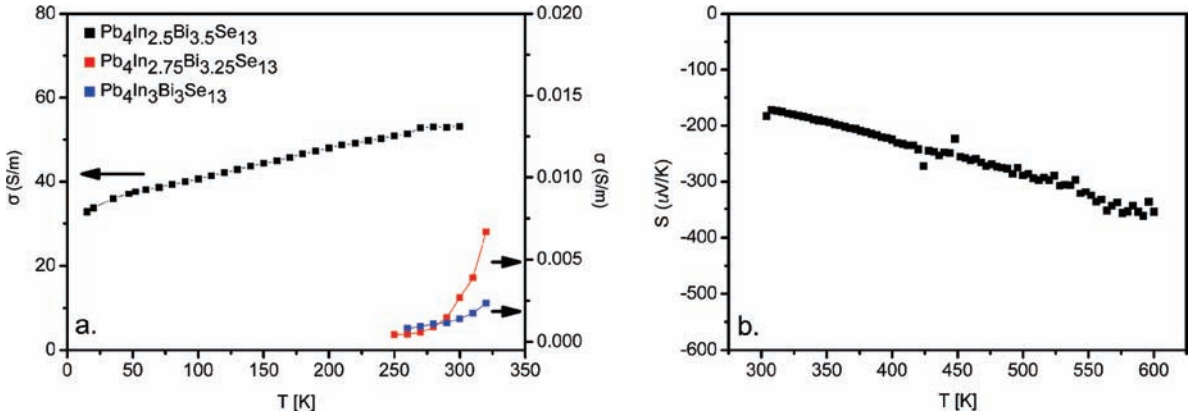

Figure 4. Temperature dependence of electrical conductivity of $Pb_4In_xBi_{6-x}Se_{13}$ (x = 2.5, 2.75, and 3.0) (a) and thermoelectric power (b) of $Pb_4In_{2.5}Bi_{3.5}Se_{13}$.

that the filled valence band corresponds to optimal In−Se bonding, whereas the Pb−Se and Bi−Se contacts are filled in antibonding states near the Fermi level that might arise from the localization of the lone-pair electrons. The model contains only In−Se interactions in sites M8−M11 corresponding to a possible composition $Pb_4In_3Bi_3Se_{13}$, which is near the upper limit of $Pb_4In_{2.8}Bi_{3.2}Se_{13}$. These results indicate that, as the number of substituted In atoms increases, the antibonding character for (M8−M11)−Se contacts near the Fermi level decreases significantly. The interatomic interactions were analyzed with ICOHP values by integrating the area of the COHP curves. For a M8−Se contact, the ICOHP for In−Se and Bi−Se are 1.03 and 0.95 eV/bond, respectively, indicative of a similar bonding strength that might be exchanged to keep the structure stable. In contrast, the other M−Se contacts (M = M9−M11) vary significantly for In−Se and Bi−Se interactions. The average ICOHP for In−Se (1.36) is greater than for Bi−Se (1.10) contact (In9−Se 1.20; In10−Se = 1.33; In11−Se1.54; Bi9−Se 1.00; Bi10−Se 1.11; Bi11−Se 1.18 eV/bond), indicative of strong bonding strength for In−Se compared with Bi−Se contact. The results indicate that the M8 site can be occupied by In or Bi, and M9−M11 sites are favored for an In atom. The condition M8 = Bi or In and M9−M11 = In yields two models $Pb_4In_2Bi_4Se_{13}$ and $Pb_4In_3Bi_3Se_{13}$, which are near the refined single-crystal data of $Pb_4In_{2.1}Bi_{3.9}Se_{13}$ and $Pb_4In_{2.8}Bi_{3.2}Se_{13}$.

The results of these theoretical calculations show a notable trend among these models. According to the

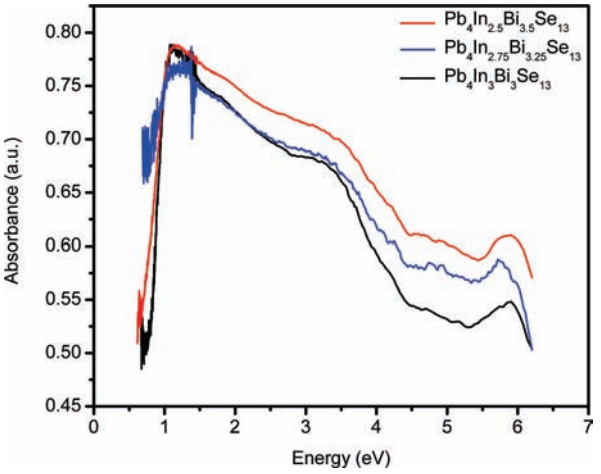

Figure 5. Diffuse reflectance spectrum of $Pb_4In_xBi_{6-x}Se_{13}$ (x = 2.5, 2.75, and 3.0).

experiments, the site composition for sites M5−M10 corresponds to mixed occupancy by In/Bi in various proportions. As the PDOS curves of In and Bi over sites M8−M11 show, the *n*s states from the Bi atom decrease as In atoms fill in the Bi site (Figure 2). As the ns^2 states from Bi make no contribution to the M−Se interactions (Figure 3), the bonding character of M−Se (M = In, Bi) and the stability of model structures are essentially the same. The results of COHP analyses indicate that the effect of replacing Bi by In is to alleviate the M−Se antibonding character to optimize their bonding interactions. These results indicate a possible phase width controlled by a varied molar ratio In/Bi in $Pb_4In_xBi_{6-x}Se_{13}$, consistent with experiment.

Physical Properties. The variation of specific electrical conductivities of $Pb_4In_xBi_{6-x}Se_{13}$ (x = 2.5, 2.75, 3) with temperature is shown in Figure 4a. All samples show that conductivity increases with increasing temperature; this dependence indicates that these compounds are semiconductors. The conductivity of a sample with x = 2.5 showed conductivity 53.18 S/m at 295 K decreasing to 32.68 S/cm at 15 K, but the electrical conductivities for samples with x = 2.75 and 3.0 are much smaller than for x = 2.5, indicating that the ratio In/Bi affects the physical properties; the compound with a small concentration of In contains a large concentration of charge carriers. Figure 4b displays the temperature dependence of the thermopower of $Pb_4In_{2.5}Bi_{3.5}Se_{13}$, which shows negative Seebeck coefficients in the range 300−600 K (∼ −180 μV/K at 300 K) with a nearly linear dependence, indicative of a *n*-type semiconductor. The Seebeck coefficients are comparable to those of Bi_2Te_3 (∼ −200 μV/K). The Seebeck coefficients for samples with x = 2.75 and 3.0 are unavailable because of their small electrical conductivity. Optical absorption spectra indicate that all compounds are semiconductors with a narrow band gap, less than 0.62 eV (Figure 5). The optical absorptions are likely due to charge-transfer transitions from filled Se-based p-orbitals to empty M-based p-orbitals. The TG-DSC measurements show similar features with exothermic maxima and mass loss beginning at 1012.0 K, 1012.3 K, and 1012.1 K for compounds with x = 2.5, 2.75, and 3, respectively, corresponding to the decomposition of those compounds (Supporting Information, Figure S3). These results were reproduced on heating the powder as synthesized in a quartz ampule under vacuum and subsequently heating to 1273 K. The X-ray powder diffraction pattern recorded after heating the sample under vacuum to 1273 K indicates that the residue contains a mixture of PbSe, Bi_2Se_3, In_2Se_3, and $Pb_2Bi_2Se_5$.

Conclusion

Quaternary selenides $Pb_4In_xM_{6-x}Se_{13}$ (M = Bi, x = 2.1−2.8; Sb, x = 2) were synthesized and characterized. The crystal structure, isostructural with that of $Pb_4In_2Bi_4S_{13}$, features a three-dimensional framework consisting of *Z*-shaped ribbon units and corner-sharing infinite one-dimensional $[InSe_4]_\infty$ chains running parallel to the *c*-axis and connected with Pb atoms to form a three-dimensional structure. For $Pb_4In_xBi_{6-x}Se_{13}$, In and Bi atoms are distributed over sites M5−M10 with a varied ratio to form a phase of width $2.1 < x < 2.8$. Measurements of electrical conductivity show decreasing resistivity with increasing temperature for $Pb_4In_xBi_{6-x}Se_{13}$. The thermopower of $Pb_4In_{2.5}Bi_{3.5}Se_{13}$ is ∼ −250(50) μV/K between 300 and 600 K, which indicates a *n*-type semiconducting property. The thermopower of $Pb_4In_{2.5}Bi_{3.5}Se_{13}$ is near that of Bi_2Te_3, but the electrical conductivity is too small for its use for thermoelectric applications. Calculations of electronic structure revealed the effect of replacing Bi by In on M−Se interactions, and the phase width is controlled by the molar ratio In/Bi in $Pb_4In_xBi_{6-x}Se_{13}$. This work shows that In not only plays an important role in the formation of the quaternary phases but also affects their physical properties.

Acknowledgment. The National Science Council (NSC94-2113-M-009-012, 94-2120-M-009-014) supported this research.

Supporting Information Available: (1) Experimental and simulated X-ray powder patterns for $Pb_4In_xBi_{6-x}Se_{13}$ (x = 2.5, 2.75, and 3.0), (2) the unit cell volume and lattice parameters as a function of Indium composition, (3) thermal analysis (TG/DSC scans) of $Pb_4In_xBi_{6-x}Se_{13}$ (x = 2.5, 2.75 and 3.0), and (4) interatomic Distances for $Pb_4In_{2.1}Bi_{3.9}Se_{13}$, $Pb_4In_{2.8}Bi_{3.2}Se_{13}$, and $Pb_4In_2Sb_4Se_{13}$. This material is available free of charge via the Internet at http://pubs.acs.org.